An Introduction to Diffusion Tensor Image Analysis

Lauren J. O'Donnell, PhD[a,b,*], Carl-Fredrik Westin, PhD[a]

KEYWORDS

• Diffusion Tensor MRI • DTI • Brain imaging
• Tractography • Review

Diffusion tensor magnetic resonance imaging (DTI) is a relatively new technology that is popular for imaging the white matter of the brain. This article provides a basic and broad overview of DTI to enable the reader to develop an intuitive understanding of these types of data, and an awareness of their strengths and weaknesses. The authors have tried to include equations for completeness, but these are not necessary for understanding the content. Wherever possible, more in-depth technical articles or books are suggested for further reading. The authors especially recommend the new diffusion MRI textbook,[1] the introductory paper on fiber tracts and tumors,[2] the white matter atlas book,[3] and the review of potential pitfalls in DTI analysis.[4] The remainder of this article addresses basic questions about DTI (the what, why, and how of DTI), followed by a discussion of issues in interpretation of DTI, and finally an overview of more advanced diffusion imaging methods and future directions.

WHY DTI? A BRIEF HISTORY OF DTI AND ITS IMPACT ON CLINICAL RESEARCH

The diffusion tensor was originally proposed for use in MRI by Peter Basser in 1994.[5,6] Before DTI, diffusion MRI[7,8] had developed from research in diffusion nuclear magnetic resonance.[9] Before the diffusion tensor model was introduced, the orientation of the axons in a tissue sample had to be known to measure anisotropic diffusion, and therefore only fixed samples could be scanned, such as the axon of the giant squid.[10] The introduction of the diffusion tensor model allowed, for the first time, a rotationally invariant description of the shape of water diffusion. The invariance to rotation was crucial because it enabled application of the DTI method to the complex anatomy of the fiber tracts in the human brain.[11] However, the diffusion tensor is not able to fully describe crossing of the fiber tracts.[12,13]

The popularity of DTI has been enormous. It has been applied to a tremendous variety of neuroscientific studies,[14–16] including schizophrenia,[17] traumatic brain injury,[18] multiple sclerosis,[19,20] autism,[21] and aging.[22] Anatomic investigations have been undertaken regarding the structure of the language network,[23,24] the asymmetry of the white matter in twins and siblings,[25] and the location, asymmetry, and variability of the fiber tracts.[26] Recent investigations have attempted to model the human "connectome" by analyzing structural versus functional brain connectivity as measured with DTI and functional MRI.[27,28] DTI has also been applied for neurosurgical planning and navigation.[29–32] A large prospective study showed that addition of preoperative DTI to

The authors acknowledge the following support: R25CA089017 (LJO), NIH R01MH074794, and NIH P41RR013218 (CFW). Thanks to Gordon Kindlmann for the eigenvalue-based formula for mode.

[a] Laboratory of Mathematics in Imaging (LMI), Department of Radiology, Brigham and Women's Hospital, Harvard Medical School, 75 Francis Street, Boston, MA 02115, USA
[b] Golby Neurosurgical Brain Mapping Laboratory, Department of Neurosurgery, Brigham and Women's Hospital, Harvard Medical School, 75 Francis Street, Boston, MA 02115, USA
* Corresponding author. Laboratory of Mathematics in Imaging (LMI), Department of Radiology, Brigham and Women's Hospital, Harvard Medical School, 75 Francis Street, Boston, MA 02115.
E-mail address: odonnell@bwh.harvard.edu

Neurosurg Clin N Am 22 (2011) 185–196
doi:10.1016/j.nec.2010.12.004

neuronavigation increased tumor resection and survival and decreased neurologic morbidity.[33]

WHAT IS DTI?

DTI is a sensitive probe of cellular structure that measures the diffusion of water molecules. The measured quantity is the diffusivity or diffusion coefficient, a proportionality constant that relates diffusive flux to a concentration gradient[8] and has units of $\frac{mm^2}{s}$. Unlike the diffusion in a glass of pure water, which would be the same in all directions (isotropic), the diffusion measured in tissue varies with direction (is anisotropic). The measured macroscopic diffusion anisotropy is the result of microscopic tissue heterogeneity.[6] In the white matter of the brain, diffusion anisotropy is primarily caused by cellular membranes, with some contribution from myelination and the packing of the axons.[11,34,35] Anisotropic diffusion can indicate the underlying tissue orientation (**Fig. 1**).

The diffusion tensor describes the diffusion of water molecules using a Gaussian model. Technically, it is proportional to the covariance matrix of a three-dimensional Gaussian distribution that models the displacements of the molecules. The tensor is a 3×3 symmetric, positive-definite matrix, and these matrix properties mean that it has three orthogonal (mutually perpendicular) eigenvectors and three positive eigenvalues. The major eigenvector of the diffusion tensor points in the principal diffusion direction (the direction of the fastest diffusion). In anisotropic fibrous tissues, the major eigenvector also defines the fiber tract axis of the tissue,[6] and thus the three orthogonal eigenvectors can be considered a local fiber coordinate system. (This interpretation is only strictly true in regions where fiber tracts do not cross, fan, or branch.) The three positive eigenvalues of the tensor $(\lambda_1, \lambda_2, \lambda_3)$ give the diffusivity in the direction of each eigenvector. Together, the eigenvectors and eigenvalues define an ellipsoid that represents an isosurface of (Gaussian) diffusion probability: the axes of the ellipsoid are aligned with the eigenvectors and their lengths are $\sqrt{2\tau\lambda_i}$.[6] **Fig. 2** shows three diffusion tensors chosen from different regions of the human brain to illustrate possible shapes of the ellipsoid.

HOW IS DTI MEASURED?

To measure diffusion using MRI, magnetic field gradients are used to create an image that is sensitized to diffusion in a particular direction. Through repeating this process of diffusion weighting in multiple directions, a three-dimensional diffusion model (the tensor) can be estimated. In simplified terms, diffusion imaging introduces extra gradient pulses whose effect "cancels out" for stationary water molecules, and causes a random phase shift for molecules that diffuse. Because of their random phase, signal from diffusing molecules is lost. This loss of signal creates darker voxels (volumetric pixels), meaning that white matter fiber tracts parallel to the gradient direction will appear dark in the diffusion-weighted image for that direction (**Fig. 3**).

Next, the decreased signal (S_k) is compared with the original signal (S_0) to calculate the diffusion tensor (D) by solving the Stejskal-Tanner Equation (1).[36] This equation describes how the signal intensity at each voxel decreases in the presence of Gaussian diffusion:

$$S_k = S_0 e^{-b\hat{g}_k^T D \hat{g}_k} \quad (1)$$

In this equation, S_0 is the original image intensity at the voxel (measured with no diffusion-sensitizing gradient) and S_k is the intensity measured after the application of the kth diffusion-sensitizing gradient in the (unit) direction $\hat{g}_k$. The product $\hat{g}_k^T D \hat{g}_k$ represents the diffusion coefficient (diffusivity) in direction $\hat{g}_k$. Because the entire set of diffusion-weighted images is used (giving many

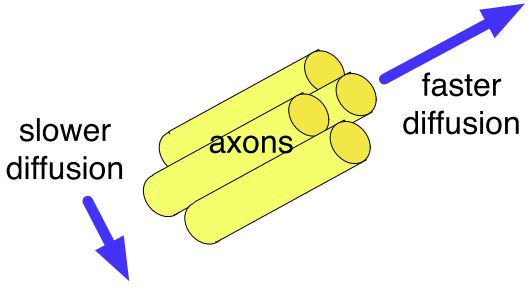

Fig. 1. Illustration of anisotropic diffusion, in the ideal case of a coherently oriented tissue. This example compares the diffusion measured parallel and perpendicular to the axons in a white matter fiber tract.

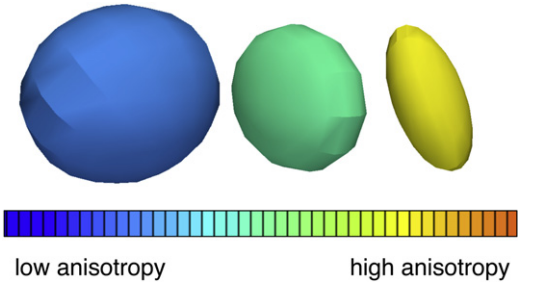

Fig. 2. Three example diffusion tensors, selected from a diffusion tensor magnetic resonance imaging scan of the human brain to illustrate differences in tensor anisotropy and orientation.

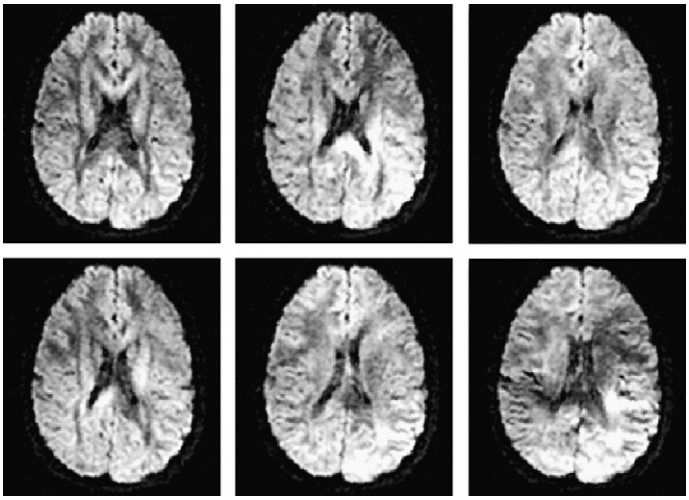

Fig. 3. Six diffusion-weighted images (the minimum number required for tensor calculation). In diffusion MRI, magnetic field gradients are used to sensitize the image to diffusion in a particular direction. The direction is different for each image, resulting in a different pattern of signal loss (*dark areas*) from anisotropic diffusion.

values for S_k and $\hat{g}_k$), this is actually a system of equations that is solved for D, the diffusion tensor. To calculate the six independent numbers in the 3×3 symmetric matrix D, at least seven images are needed: six diffusion-weighted images from six gradient directions (giving six values for S_k) plus one baseline image (giving S_0). However, in clinical research today, a higher number of images are almost always used. The above system of equations can be solved via the least squares method at each voxel.

Equation (1) also contains b, LeBihan's[9] factor describing the pulse sequence, gradient strength, and physical constants. The b-factor is near 0 $\frac{s}{mm^2}$ for the image S_0, which is T2-weighted, and the b-factor is near 1000 $\frac{s}{mm^2}$ for the diffusion-weighted images S_k in DTI. For rectangular gradient pulses, the b-factor is defined by $b = \gamma^2\delta^2(\Delta - \frac{\delta}{3})|g|^2$, where γ is the proton gyromagnetic ratio (42 MHz/Tesla), $|g|$ is the strength of the diffusion sensitizing gradient pulses, δ is the duration of the diffusion gradient pulses, and

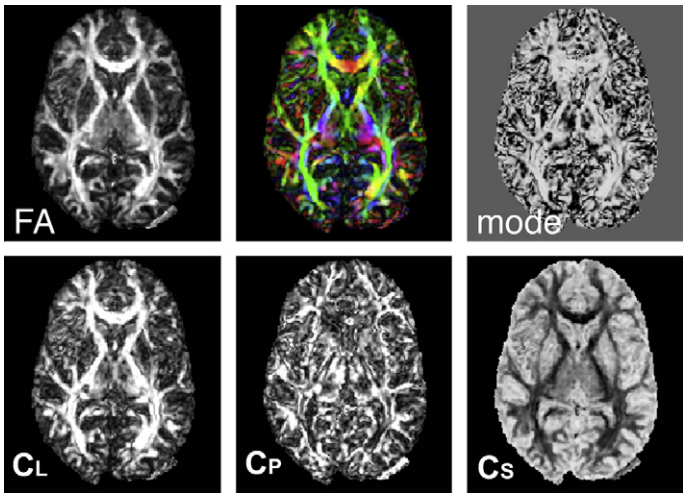

Fig. 4. Scalar measures derived from DTI include FA, mode, C_L, C_P, and C_S. Also shown (*top row, middle*) is a mapping of the major eigenvector orientation to colors. See the text for more information about the definition of these measures.

Δ is the time between diffusion gradient RF pulses.[37]

Information on the MR physics of DTI[8] and more information on the tensor calculation process[5,37] are provided elsewhere. Goodlett and colleagues[38] provide a comparison of tensor calculation methods (including least squares and weighted least squares) in the presence of noise.

HOW IS DTI DISPLAYED?

DTI is usually displayed through condensing the information contained in the tensor (**Fig. 4**) into either one number (a scalar), or four (to give an RGB color and a brightness value). The diffusion tensor can also be viewed using glyphs, which are small three-dimensional representations of the major eigenvector or whole tensor. Finally, DTI is often viewed through estimating the course of white matter tracts through the brain using a process called *tractography*.

Scalars Derived from DTI

This section describes commonly used scalar quantities, which can be divided into two categories: diffusion magnitude measures and anisotropy measures. The eigenvalues of the symmetric, positive-definite diffusion tensor D are referred to using $\lambda_1 \geq \lambda_2 \geq \lambda_3 \geq 0$. Pierpaoli and colleagues[11] originally measured and compared several scalar measures, and the eigenvalues, in different regions of the human brain.

Measures of diffusion magnitude

The simplest and possibly most useful scalar is the average of the tensor's eigenvalues. This average may be referred to as the *mean diffusivity* (MD)[39]; the bulk mean diffusivity ($\langle D \rangle$)[40]; or the apparent diffusion coefficient (ADC) map. In clinical imaging, ADC maps may be measured using fewer diffusion gradients than needed for the tensor. A similar quantity to the MD is the sum of the eigenvalues, called the *trace* of the tensor.

The trace and MD relate to the total amount of diffusion in a voxel, which is related to the amount of water in the extracellular space. The trace is clinically useful in early stroke detection because it is sensitive to the initial cellular swelling (cytotoxic edema) that restricts diffusion.[41] In the normal human brain, the trace is high in cerebrospinal fluid, around $9.6 \times 10^{-3}\frac{mm^2}{s}$, and relatively constant in normal brain parenchyma (white and gray matter), between $1.95 \times 10^{-3}\frac{mm^2}{s}$ and $2.2 \times 10^{-3}\frac{mm^2}{s}$.[11] For comparison, the self-diffusion coefficient of water (the diffusivity measured in pure water without any tissue) at a body temperature of 37°C is $3 \times 10^{-3}\frac{mm^2}{s}$,[42] which would give a trace of $9 \times 10^{-3}\frac{mm^2}{s}$. The MD and trace measured in ventricles or in edema can be higher than in water because of fluid flow or enhanced perfusion, respectively.[7]

Measures of diffusion anisotropy

Tensor anisotropy measures are ratios of the eigenvalues that are used to quantify the shape of the diffusion. These measures are useful for describing the amount of tissue organization and for locating voxels likely to contain a single white matter tract (without crossing or fanning). The following measures are normalized and all range from 0 to 1, except for the mode, which ranges from –1 to +1.

The fractional anisotropy (FA)[43] is the most widely used anisotropy measure. Its name comes from the fact that it measures the fraction of the diffusion that is anisotropic. This measure can be considered the difference of the tensor ellipsoid's shape from that of a perfect sphere. FA is basically a normalized variance of the eigenvalues:

$$FA = \frac{1}{\sqrt{2}} \frac{\sqrt{(\lambda_1 - \hat{\lambda})^2 + (\lambda_2 - \hat{\lambda})^2 + (\lambda_1 - \hat{\lambda})^2}}{\sqrt{\lambda_1^2 + \lambda_2^2 + \lambda_3^2}} \quad (2)$$

where $\hat{\lambda}$ is the mean diffusivity. FA is often considered a measure of white matter integrity, although changes in FA may be caused by many factors.

Three intuitive measures are C_L, C_P, and C_S, which are the linear, planar, and spherical shape measures.[37,44] They describe whether the shape of diffusion is similar to a cigar (linear), pancake (planar), or sphere (spherical).

$$C_L = \frac{\lambda_1 - \lambda_2}{\lambda_1} \quad (3)$$

$$C_P = \frac{\lambda_2 - \lambda_3}{\lambda_1} \quad (4)$$

$$C_S = \frac{\lambda_3}{\lambda_1} \quad (5)$$

In voxels with high planar or spherical measure, the principal eigenvector will not always match an underlying fiber tract direction (where tracts cross the eigenvector may point to neither one). However, if the largest eigenvalue is much larger than the other two eigenvalues, the linear measure will be large, indicating the presence of a single fiber tract. These measures can be normalized by λ_1, by the trace, or by $\sqrt{\lambda_1^2 + \lambda_2^2 + \lambda_3^2}$.

Although FA measures how far the tensor is from a sphere, another complementary measure discriminates between linear and planar anisotropy. This information is given by the mode,

a quantity that is mathematically orthogonal to the FA measure and relates to the skewness of the eigenvalues.[45]

mode

$$= \frac{(-\lambda_1 - \lambda_2 + 2\lambda_3)(2\lambda_1 - \lambda_2 - \lambda_3)(-\lambda_1 + 2\lambda_2 - \lambda_3)}{2\left(\lambda_1^2 + \lambda_2^2 + \lambda_3^2 - \lambda_1\lambda_2 - \lambda_1\lambda_3 - \lambda_2\lambda_3\right)^{3/2}} \quad (6)$$

The parallel diffusivity measure, also called the *axial diffusivity*, is equal to the largest eigenvalue. The perpendicular diffusivity measure, also called the *radial diffusivity*, is equal to the average of the two smaller eigenvalues. These measures are interpreted as diffusivity parallel and perpendicular to a white matter fiber tract, and therefore make the most sense in regions of coherently oriented axons with no fiber crossings.

Often in scientific studies, the reported measures from the diffusion tensor are not independent. However, complete sets of orthogonal (mathematically independent) scalars have been defined.[45,46]

Colors Derived from DTI

Another type of image can represent the major eigenvector field using a mapping to colors (**Fig. 5**). The color scheme most commonly used to represent the orientation of the major eigenvector works as follows: blue is superior–inferior, red is left–right, and green is anterior–posterior.[47] To enhance visualization of the white matter and suppress information outside of it, the brightness of the color is usually controlled by tensor anisotropy (FA).

Glyphs Derived from DTI

Small three-dimensional objects called *glyphs* can be used to display information from each tensor eigensystem. Example glyphs include "sticks" representing the orientation of the major eigenvector, ellipsoids related to the diffusion isoprobability surfaces,[6] and superquadric tensor glyphs.[48]

Tractography

The word *tractography* refers to any method for estimating the trajectories of the fiber tracts in the white matter. Ciccarelli and colleagues[15] provide a clinical and technical overview of tractography in neurologic disorders. Tractography techniques, including explanations of common tractography artifacts and a comparison of methods, are reviewed elsewhere.[49,50] Many methods have been proposed for tractography, and the results will vary enormously depending on the chosen method.

The most common approach is streamline tractography (**Fig. 6**),[51–54] which is closely related to an earlier method for visualization of tensor fields, known as *hyperstreamlines*.[55] This method produces as output discrete curves or trajectories that are also referred to by terms such as *tracts*, *fibers*, and *traces*. The streamline tract-tracing approach works by successively stepping in the direction of the principal eigenvector (the direction of fastest diffusion). The eigenvectors are thus tangent to the trajectory that is produced. A fixed step size of 1 mm or less (smaller than a voxel) is generally used for DTI data.

Several computational methods can be used to perform basic streamline tractography, including Euler's method (following the eigenvector or tangent for a fixed step size), second-order Runge-Kutta (also known as the *midpoint method*, in which the tangent is followed for half a step, then a new tangent is calculated at the midpoint of the interval and used to take the full step), and

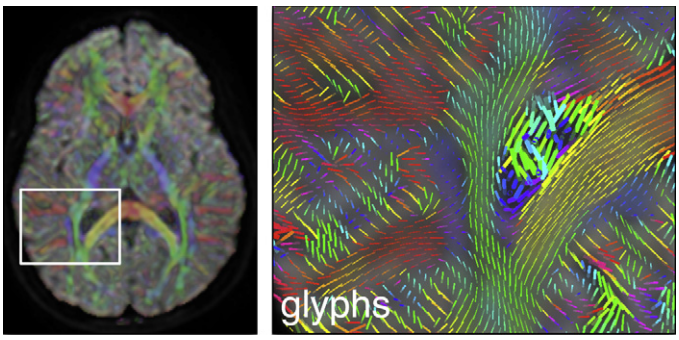

Fig. 5. An example using glyphs and colors for diffusion tensor magnetic resonance imaging visualization. On the left an axial image plane, showing the average diffusion-weighted image with semitransparent color overlay indicating the major eigenvector orientation, and a white square indicating the zoomed-in area (*right image*). In both images, the color red indicates right–left orientation, blue is superior–inferior, and green is anterior–posterior. The right image contains glyphs representing major eigenvector orientations (and scaled by the largest eigenvalue) in the region of the corpus callosum (*yellow* and *red*) and right lateral ventricle. The cingulum can be seen in blue, and the posterior limb of the internal capsule in green.

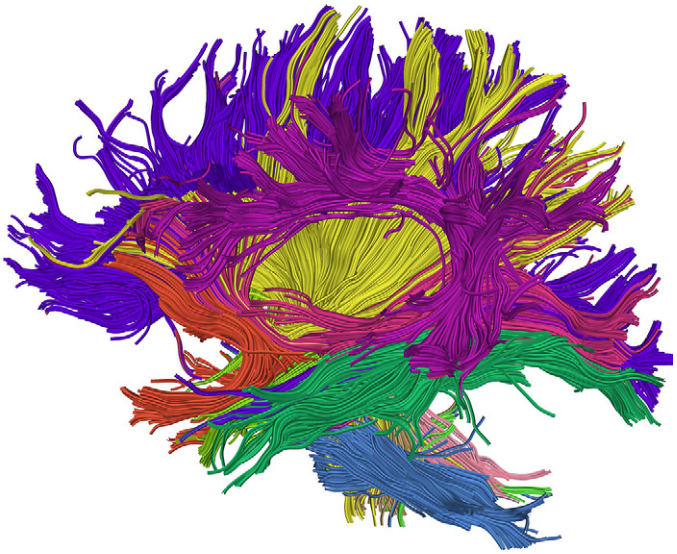

Fig. 6. Whole-brain streamline DTI tractography. Colors were assigned automatically according to an atlas-based tractography segmentation method. (*Data from* O'Donnell LJ, Westin CF. Automatic tractography segmentation using a high-dimensional white matter atlas. IEEE Trans Med Imaging 2007;26:1562–75.)

fourth-order Runge-Kutta (in which the weighted average of four estimated tangents to the curve is used when taking each step).[56] Basser and colleagues[51] and Conturo and colleagues[52] explored application of the Euler and Runge-Kutta methods to white matter tractography. Another popular method is called fiber assessment by continuous tracking.[53] Some related methods attempt to introduce inertia when tracking through regions of planar anisotropy (likely fiber crossings). These methods modulate the incoming tangent direction by the tensor instead of directly using the major eigenvector of the tensor.[37,54,57,58]

Processing DTI data to display fiber tracts of interest requires expert knowledge or an automatic algorithm. After performing streamline tractography, the fiber trajectories of interest can be interactively selected through virtual dissection, in which inclusion/exclusion regions are defined and used to select trajectories.[3,59,60] Automated methods for atlas-based tractography segmentation, which use prior knowledge to select trajectories, have also been developed.[61–67]

In addition to streamline tractography, many other methods are available,[49,50] including probabilistic tractography that outputs connection strengths or probabilities,[68,69] optimization methods that use graph theory or physical models,[70,71] region-growing and wavefront evolution methods,[72] tractography using advanced models for fiber crossings,[73–76] and tractography meta-analysis methods that perform clustering or fit more sophisticated tract models.[61,77–79]

Tractography methods can produce false-positive and -negative results (discussed in next section); however, clinical validations of streamline tractography have shown accurate reconstructions (true-positive results). Tract end points, especially of the corticospinal or motor tract, have been compared with electrocortical stimulation during neurosurgery[80,81] with good correspondence. In a study of 238 neurosurgical patients with gliomas involving the motor tract who were randomized to study or control groups, DTI was shown to increase survival and reduce postoperative motor deficits.[33]

ISSUES IN INTERPRETING DTI DATA

This section presents two issues that are relevant to the clinical interpretation or meaning of the DTI data. Jones and Cercignani[4] have provided a more thorough discussion, including additional information about scanning and processing pitfalls.

Scale of Diffusion Measurements Versus Axons

The measured diffusion effects are averaged over a voxel (three-dimensional pixel), complicating the biophysical interpretation of the diffusion tensor.[40,82] For example, in scientific studies FA is often interpreted as "white matter integrity"; however, many factors (eg, cell death, change in myelination, increase in extracellular or

Table 1
The scale of diffusion tensor magnetic resonance imaging and the brain: neuron sizes and quantities, and water diffusion times and distances

Quantity	Measurement	References
Axon packing density (pyramidal tract)	60,000–70,000/mm^2	11
Axon packing density (corpus callosum)	338,000/mm^2	11
Axon diameter (pyramidal tract)	26 μm	11
Axon diameters in central nervous system	0.2–20 μm	83
Neuron cell body diameter	≥50 μm	83
Typical voxel size in diffusion MRI	2.5 × 2.5 × 2.5 mm	
Typical diffusion time in diffusion tensor magnetic resonance imaging	30–100 ms	34,42
Mean water diffusion distance	1–15 μm (in 50–100 ms)	42
Number of neurons in human brain	100 billion (10^{11})	83
Synaptic connections per axon	Up to 1,000	83

intracellular water) may cause changes in FA. Overall, this difficulty in interpreting DTI is because the scale at which diffusion is measured with DTI is very different from the size scale of individual axons. To illustrate the complexity of the human brain and the size/time scales of the diffusion imaging experiment, **Table 1** lists relevant quantities, such as the number of neurons in the brain (10^{11}) and the distance over which water diffuses during an imaging experiment (1–15 μm, a distance similar to the diameter of an axon).

False-Positive or -Negative Tractography

Because the tensor model is only able to represent one major fiber direction in a voxel, DTI tractography can be confounded by regions of crossing fibers, as shown schematically in **Fig. 7**. A significant fraction of white matter voxels in the brain contain multiple fiber bundles oriented in different directions, where the diffusion tensor model is not reliable.[73] Other factors can confound tractography. Partial volume effects, in which two types of tissue are present in a voxel, can produce a tensor that represents neither tissue well.[82] Also, crossing, "kissing," and "fanning" fiber tracts[12] are not represented well at the voxel level by the diffusion tensor. Finally, in standard streamline tractography, all decisions are made locally, and therefore errors can accumulate.

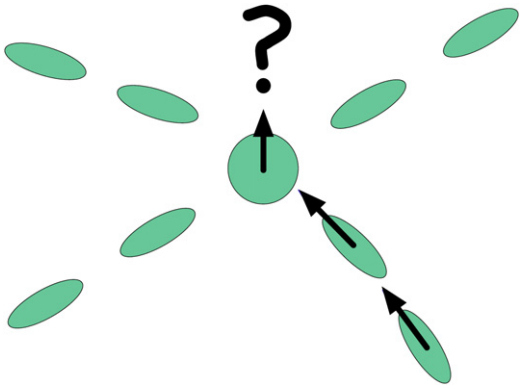

Fig. 7. The major eigenvector may not be aligned with a fiber tract in the case of crossing fibers.

These issues may cause false-positive and -negative connections (**Figs. 8** and **9**). Common false-positive connections include trajectories from the corona radiata that cross the corpus callosum, and trajectories from the corona radiata that cross at the pons and ascend in the corona radiata of the other hemisphere. Common false-negatives with DTI tractography are the lateral lip/hand connections of the corticospinal tract[49,73] and lateral connections of the corpus callosum.[74]

The particular errors depend strongly on the tractography algorithm used, and on the type of diffusion data used (DTI vs higher-order models). However, no perfect method exists, and perfect tractography is unlikely to be possible because even perfect diffusion MRI data would not solve the peak selection problem. At each step, a direction must be chosen to follow for the next step, and with a more detailed model than the tensor, this requires some logical heuristic, such as choosing the closest direction to the current direction.

ADVANCES BEYOND THE DIFFUSION TENSOR

New diffusion models, scanning paradigms, and analysis methods are continually being developed for diffusion MRI.

High angular resolution diffusion imaging (HARDI) includes methods that acquire diffusion data using many more than 6 diffusion directions (eg, ≥ 32).[84] These methods generally use a higher

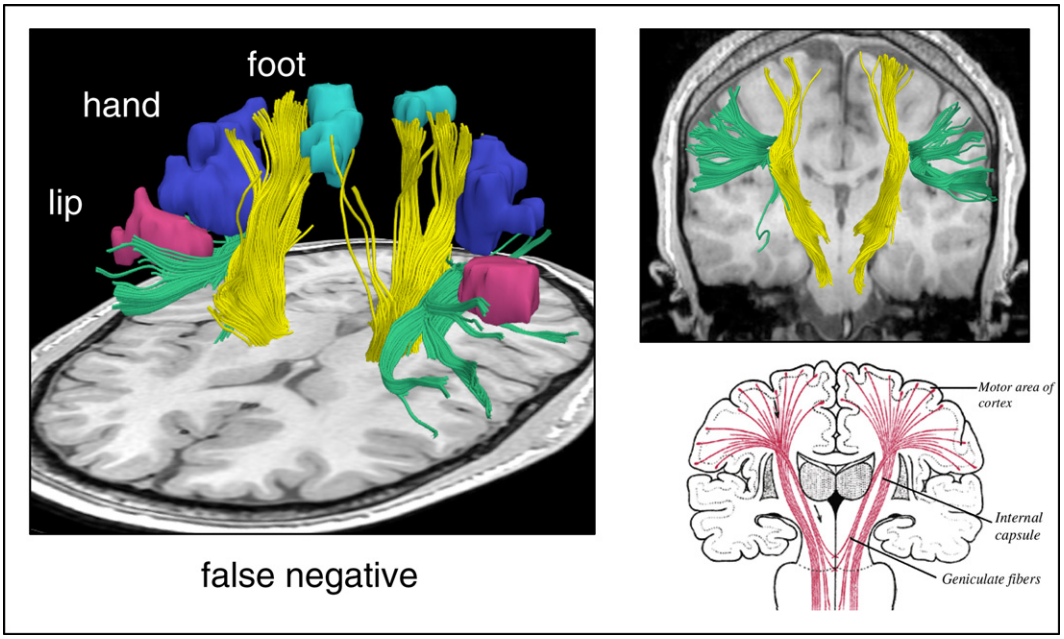

Fig. 8. Example false-negative streamline tractography error. The motor fibers (*yellow*) do not reach all functional magnetic resonance (fMRI) motor activations (*aqua*, *blue*, and *pink*) due to the presence of the superior longitudinal fasciculus (*green*) that runs perpendicular to the motor tract. In the right column are coronal views of the typical streamline tractography result (*top*) and expected anatomy (*bottom*).

b-value than the standard 1000 for DTI, or multiple b-values (multiple "shells" of data). Multi-shell acquisitions enable description of the full diffusion function using measures such as displacement, zero-probability, and kurtosis that are highly sensitive to myelin.[85,86] Another type of multiple b-value acquisition is diffusion spectrum imaging (DSI).[87] Diffusion models that go beyond DTI have been proposed to extract important biomarkers, such as compartmentalization[13,82,88,89] and axon diameter.[90] Higher-rank tensor models have been proposed to extend DTI.[91] Use of multiple pairs of diffusion gradients (double pulsed field gradient diffusion MRI) has been shown to increase sensitivity to small size scales.[92,93] Diffusion MRI data analysis has benefited from the introduction of novel tractography methods, many types of white matter atlas,[61–67] advanced tract-based quantification methods,[77–79,94] new visualization methods,[95] and new scalar measures.[45,96]

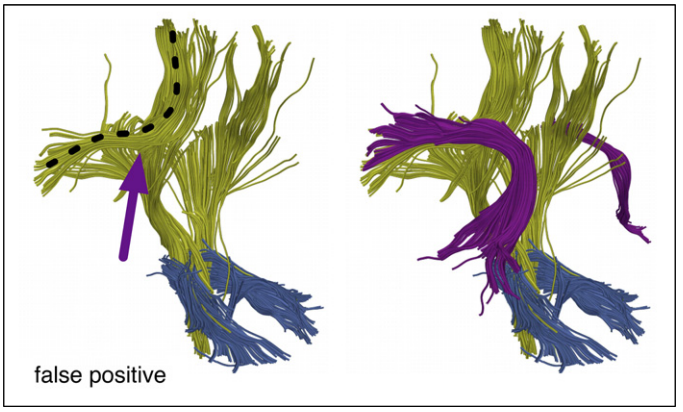

Fig. 9. False-positive streamline tractography error. In the left image, fibers (*yellow with black dotted line*) have traced parts of two anatomic structures by incorrectly crossing from one to the other (*at arrow*). In the right image, both structures (arcuate fasciculus in magenta and corona radiata in *yellow*) can be seen.

SUMMARY

DTI is an increasingly prevalent and popular imaging modality that has been applied to numerous scientific studies and clinical problems since its invention a little more than 15 years ago. The field is expected to benefit from many future advances in diffusion imaging and analysis.

REFERENCES

1. Johansen-Berg H, Behrens Timothy EJ, editors. Diffusion MRI: from quantitative measurement to in-vivo neuroanatomy. 1st edition. Elsevier Academic Press; May 4, 2009.
2. Jellison BJ, Field AS, Medow J, et al. Diffusion tensor imaging of cerebral white matter: a pictorial review of physics, fiber tract anatomy, and tumor imaging patterns. AJNR Am J Neuroradiol 2004;25:356–69.
3. Oishi K, Faria AV, Zijl Peter CM, et al. MRI atlas of human white matter. Elsevier Academic Press; 2010.
4. Jones DK, Cercignani M. Twenty-five pitfalls in the analysis of diffusion MRI data. NMR Biomed 2010; 23:803–20.
5. Basser PJ, Mattiello J, LeBihan D. Estimation of the effective self-diffusion tensor from the NMR spin echo. J Magn Reson B 1994;103:247–54.
6. Basser PJ, Mattiello J, LeBihan D. MR diffusion tensor spectroscopy and imaging. Biophys J 1994;66:259–67.
7. Le Bihan D, Breton E, Lallemand D, et al. MR imaging of intravoxel incoherent motions: application to diffusion and perfusion in neurologic disorders. Radiology 1986;161:401–7.
8. Le Bihan D, Basser PJ. Diffusion and perfusion magnetic resonance imaging: applications to functional MRI chapter. Molecular diffusion and nuclear magnetic resonance. Raven Press; 1995. p. 5–17.
9. LeBihan D. Molecular diffusion nuclear magnetic resonance imaging. Magn Reson Q 1991;7:1–30.
10. Beaulieu C, Allen PS. Water diffusion in the giant axon of the squid: implications for diffusion-weighted MRI of the nervous system. Magn Reson Med 1994;32: 579–83.
11. Pierpaoli C, Jezzard P, Basser PJ, et al. Diffusion tensor MR imaging of the human brain. Radiology 1996;201:637.
12. Wiegell MR, Larsson HB, Wedeen VJ. Fiber crossing in human brain depicted with diffusion tensor MR imaging1. Radiology 2000;217:897–903.
13. Tuch DS. High angular resolution diffusion imaging reveals intravoxel white matter fiber heterogeneity. Magn Reson Med 2002;48:577–82.
14. Horsfield MA, Jones DK. Applications of diffusion-weighted and diffusion tensor MRI to white matter diseases—a review. NMR Biomed 2002;15:570–7.
15. Ciccarelli O, Catani M, Johansen-Berg H, et al. Diffusion-based tractography in neurological disorders: concepts, applications, and future developments. Lancet Neurol 2008;7:715–27.
16. Assaf Y, Pasternak O. Diffusion tensor imaging (DTI)-based white matter mapping in brain research: a review. J Mol Neurosci 2008;34:51–61.
17. Kubicki M, McCarley R, Westin CF, et al. A review of diffusion tensor imaging studies in schizophrenia. J Psychiatr Res 2007;41:15–30.
18. Maller JJ, Thomson RH, Lewis PM, et al. Traumatic brain injury, major depression, and diffusion tensor imaging: making connections. Brain Res Rev 2010; 64:213–40.
19. Inglese M, Bester M. Diffusion imaging in multiple sclerosis: research and clinical implications. NMR Biomed 2010;23:865–72.
20. Filippi M, Agosta F. Imaging biomarkers in multiple sclerosis. J Magn Reson Imaging 2010;31:770–88.
21. Lange N, DuBray MB, Lee JE, et al. Atypical diffusion tensor hemispheric asymmetry in autism. Autism Res 2010;3(6):350–8.
22. Westlye LT, Walhovd KB, Dale AM, et al. Life-span changes of the human brain white matter: diffusion tensor imaging (DTI) and volumetry. Cereb Cortex 2010;20:2055–68.
23. Catani M, Jones DK, ffytche DH. Perisylvian language networks of the human brain. Ann Neurol 2005;57:8–16.
24. Glasser MF, Rilling JK. DTI tractography of the human brain's language pathways. Cereb Cortex 2008;18:2471–82.
25. Jahanshad N, Lee AD, Barysheva M, et al. Genetic influences on brain asymmetry: a DTI study of 374 twins and siblings. Neuroimage 2010;52:455–69.
26. Schotten Thiebaut M, Ffytche DH, Bizzi A, et al. Atlasing location, asymmetry and inter-subject variability of white matter tracts in the human brain with MR diffusion tractography. Neuroimage 2011; 54:49–59.
27. Sporns O, Tononi G, Kotter R. The human connectome: a structural description of the human brain. PLoS Comput Biol 2005;1:e42.
28. Honey CJ, Sporns O, Cammoun L, et al. Predicting human resting-state functional connectivity from structural connectivity. Proc Natl Acad Sci U S A 2009;106(6):2035–40.
29. Talos IF, O'Donnell L, Westin CF, et al. Diffusion tensor and functional MRI fusion with anatomical MRI for image-guided neurosurgery. Presented at: Sixth International Conference on Medical Image Computing and Computer-Assisted Intervention-MICCAI; November 15–18, 2003; Montreal, Canada; 407–15.
30. Nimsky C, Ganslandt O, Fahlbusch R. Implementation of fiber tract navigation. Neurosurgery 2006; 58:ONS-292–303.
31. Bello L, Gambini A, Castellano A, et al. Motor and language DTI fiber tracking combined with

intraoperative subcortical mapping for surgical removal of gliomas. Neuroimage 2008;39:369–82.
32. Golby AJ, Kindlmann G, Norton I, et al. Interactive diffusion tensor tractography visualization for neurosurgical planning. Neurosurgery 2011;68(2):496–505.
33. Wu JS, Zhou LF, Tang WJ, et al. Clinical evaluation and follow-up outcome of diffusion tensor imaging-based functional neuronavigation: a prospective, controlled study in patients with gliomas involving pyramidal tracts. Neurosurgery 2007;61:935.
34. Beaulieu C. The basis of anisotropic water diffusion in the nervous system—a technical review. NMR Biomed 2001;15:435–55.
35. Sen PN, Basser PJ. A model for diffusion in white matter in the brain. Biophys J 2005;89:2927–38.
36. Basser PJ. Inferring microstructural features and the physiological state of tissues from diffusion-weighted images. NMR Biomed 1995;8:333–44.
37. Westin CF, Maier SE, Mamata H, et al. Processing and visualization of diffusion tensor MRI. Med Image Anal 2002;6:93–108.
38. Goodlett C, Fletcher PT, Lin W, et al. Quantification of measurement error in DTI: theoretical predictions and validation. In: Proceedings of the 10th International Conference on Medical image Computing and Computer-Assisted Intervention—Volume Part I. Springer-Verlag; 2007:10–7.
39. Le Bihan D, Mangin JF, Poupon C, et al. Diffusion tensor imaging: concepts and applications. J Magn Reson Imaging 2001;13:534–46.
40. Basser PJ, Jones DK. Diffusion-tensor MRI: theory, experimental design and data analysis—a technical review. NMR Biomed 2002;15:456–67.
41. Schlaug G, Siewert B, Benfield A, et al. Time course of the apparent diffusion coefficient (ADC) abnormality in human stroke. Neurology 1997;49:113–9.
42. Le Bihan D. Looking into the functional architecture of the brain with diffusion MRI. Nat Rev Neurosci 2003;4:469–80.
43. Basser PJ, Pierpaoli C. Microstructural and physiological features of tissues elucidated by quantitative-diffusion-tensor MRI. J Magn Reson B 1996;111:209–19.
44. Westin CF, Peled S, Gudbjartsson H, et al. Geometrical diffusion measures for MRI from tensor basis analysis. In: ISMRM 97 Vancouver, Canada; 1997: p. 1742.
45. Ennis DB, Kindlmann G. Orthogonal tensor invariants and the analysis of diffusion tensor magnetic resonance images. Magn Reson Med 2006;55:136–46.
46. Kindlmann G, Ennis DB, Whitaker RT, et al. Diffusion tensor analysis with invariant gradients and rotation tangents. IEEE Trans Med Imaging 2007;26:1483–99.
47. Pajevic S, Pierpaoli C. Color schemes to represent the orientation of anisotropic tissues from diffusion tensor data: application to white matter fiber tract mapping in the human brain. Magn Reson Med 1999;42(3):526–40. [Erratum in: Magn Reson Med 2000;43(6):921].
48. Kindlmann G. Superquadric tensor glyphs. In: IEEE Transactions on Visualization and Computer Graphics/EG Symposium on Visualization; 2004. p. 147–54.
49. Jones DK. Studying connections in the living human brain with diffusion MRI. Cortex 2008;44:936–52.
50. Lazar M. Mapping brain anatomical connectivity using white matter tractography. NMR Biomed 2010;23:821–35.
51. Basser PJ, Pajevic S, Pierpaoli C, et al. In vivo fiber tractography using DT–MRI data. Magn Reson Med 2000;44:625–32.
52. Conturo TE, Lori NF, Cull TS, et al. Tracking neuronal fiber pathways in the living human brain. Neurobiology 1999;96:10422–7.
53. Mori S, Crain BJ, Chacko VP, et al. Three dimensional tracking of axonal projections in the brain by magnetic resonance imaging. Ann Neurol 1999;45:265–9.
54. Westin CF, Maier SE, Khidhir B, et al. Image processing for diffusion tensor magnetic resonance imaging. In: Medical Image Computing and Computer-Assisted Intervention, Lecture Notes in Computer Science; 1999. p. 441–52.
55. Delmarcelle T, Hesselink L. Visualization of second order tensor fields and matrix data. In: Proceedings of IEEE Visualization '92; 1992. p. 316–23.
56. Press WH, Teukolsky SA, Vetterling WT, et al. Numerical recipes in C: the art of scientific computing. Cambridge University Press; 1992.
57. Weinstein D, Kindlmann G, Lundberg E. Tensorlines: advection-diffusion based propagation through diffusion tensor fields. In: Proceedings of IEEE Visualization '99; 1999. p. 249–53.
58. Lazar M, Weinstein DM, Tsuruda JS, et al. White matter tractography using diffusion tensor deflection. Hum Brain Mapp 2003;18:306–21.
59. Conturo TE, Lori NF, Cull TS, et al. Tracking neuronal fiber pathways in the living human brain. Proc Natl Acad Sci U S A 1999;96:10422.
60. Catani M, Howard RJ, Pajevic S, et al. Virtual in vivo interactive dissection of white matter fasciculi in the human brain. Neuroimage 2002;17:77–94.
61. O'Donnell LJ, Westin CF. Automatic tractography segmentation using a high-dimensional white matter atlas. IEEE Trans Med Imaging 2007;26:1562–75.
62. Goodlett C, Davis B, Jean R, et al. Improved correspondence for DTI population studies via unbiased atlas building. Proceedings of Med Image Comput Comput Assist Interv 2006;9(Pt 2):260–67.
63. Yushkevich PA, Zhang H, Simon T, et al. Gee structure-specific statistical mapping of white matter tracts. Neuroimage 2008;41(2):448–61.

64. Mori S, Oishi K, Jiang H, et al. Stereotaxic white matter atlas based on diffusion tensor imaging in an ICBM template. Neuroimage 2008;40:570–82.
65. Maddah M, Grimson WE, Warfield SK, et al. A unified framework for clustering and quantitative analysis of white matter fiber tracts. Med Image Anal 2008;12:191–202.
66. Catani M, Schotten T. A diffusion tensor imaging tractography atlas for virtual in vivo dissections. Cortex 2008;44:1105–32.
67. Hagler DJ Jr, Ahmadi ME, Kuperman J, et al. Automated white-matter tractography using a probabilistic diffusion tensor atlas: application to temporal lobe epilepsy. Hum Brain Mapp 2009;30:1535.
68. Behrens TE, Woolrich MW, Jenkinson M, et al. Characterisation and propagation of uncertainty in diffusion weighted MR imaging. Magn Reson Med 2003;50:1077–88.
69. Behrens TE, Johansen-Berg H, Woolrich MW, et al. Non-invasive mapping of connections between human thalamus and cortex using diffusion imaging. Nat Neurosci 2003;6:750–7.
70. O'Donnell L, Haker S, Westin CF. New approaches to estimation of white matter connectivity in diffusion tensor MRI: elliptic PDEs and Geodesics in a tensor-warped space. In: Dohi T, Kikinis R, editors. Medical Image Computing and Computer-Assisted Intervention (MICCAI). Tokyo (Japan): 2002. p. 459–66.
71. Kreher BW, Mader I, Kiselev VG. Gibbs tracking: a novel approach for the reconstruction of neuronal pathways. Magn Reson Med 2008;60:953–63.
72. Melonakos J, Mohan V, Niethammer M, et al. Finsler tractography for white matter connectivity analysis of the cingulum bundle. In: Proceedings of the 10th International Conference on Medical Image Computing and Computer-Assisted Intervention—Volume Part IMICCAI'07. Berlin, Heidelberg: Springer-Verlag; 2007:36–43.
73. Behrens TE, Berg HJ, Jbabdi S, et al. Probabilistic diffusion tractography with multiple fibre orientations: what can we gain? Neuroimage 2007;34: 144–55.
74. Wedeen VJ, Wang RP, Schmahmann JD, et al. Diffusion spectrum magnetic resonance imaging (DSI) tractography of crossing fibers. Neuroimage 2008; 41:1267–77.
75. Qazi AA, Radmanesh A, O'Donnell L, et al. Resolving crossings in the corticospinal tract by two-tensor streamline tractography: method and clinical assessment using fMRI. Neuroimage 2008;47(Suppl 2): T98–106.
76. Malcolm JG, Shenton ME, Rathi Y. Filtered multitensor tractography. IEEE Trans Med Imaging 2010;29:1664–75.
77. Yushkevich PA, Zhang H, Simon TJ, et al. Structure-specific statistical mapping of white matter tracts. Neuroimage 2008;41:448–61.
78. O'Donnell L, Golby AJ, Westin CF. Tract-based morphometry for white matter group analysis. Neuroimage 2009;45:832–44.
79. Sherbondy A, Rowe M, Alexander D. MicroTrack: an algorithm for concurrent projectome and microstructure estimation. In: Jiang T, Navab N, Pluim J, et al, editors. Medical image computing and computer-assisted intervention: MICCAI 2010. Springer; 2010. p. 183–90.
80. Kamada K, Todo T, Ota T, et al. The motor-evoked potential threshold evaluated by tractography and electrical stimulation. J Neurosurg 2009;111:785–95.
81. Bello L, Castellano A, Fava E, et al. Intraoperative use of diffusion tensor imaging fiber tractography and subcortical mapping for resection of gliomas: technical considerations. Neurosurg Focus 2010;28:E6.
82. Alexander AL, Hasan KM, Lazar M, et al. Analysis of partial volume effects in diffusion-tensor MRI. Magn Reson Med 2001;45:770–80.
83. Kandel Eric R, Schwartz James H, Jessel Thomas M. Principles of neural science. McGraw-Hill; 2000.
84. Tuch DS. Q-ball imaging. Magn Reson Med 2004; 52:1358–72.
85. Bar-Shir A, Duncan ID, Cohen Y. QSI and DTI of excised brains of the myelin-deficient rat. Neuroimage 2009;48:109–16.
86. Wu EX, Cheung MM. MR diffusion kurtosis imaging for neural tissue characterization. NMR Biomed 2010;23:836–48.
87. Wedeen VJ, Hagmann P, Tseng WI, et al. Mapping complex tissue architecture with diffusion spectrum magnetic resonance imaging. Magn Reson Med 2005;54:1377–86.
88. Assaf Y, Basser PJ. Composite hindered and restricted model of diffusion (CHARMED) MR imaging of the human brain. Neuroimage 2005;27: 48–58.
89. Peled S, Friman O, Jolesz F, et al. Geometrically constrained two-tensor model for crossing tracts in DWI. Magn Reson Imaging 2006;24:1263–70.
90. Assaf Y, Blumenfeld-katzir T, Yovel Y, et al. AxCaliber: a method for measuring axon diameter distribution from diffusion MRI. Magn Reson Med 2008;59: 1347–54.
91. Ozarslan E, Vemuri Baba C, Mareci Thomas H. Higher rank tensors in diffusion MRI. In: Weickert J, Hagen H, editors. Visualization and processing of tensor fields. Mathematics and visualization. Berlin: Springer; 2006. p. 177–87.
92. Ozarslan E, Basser PJ. Microscopic anisotropy revealed by NMR double pulsed field gradient experiments with arbitrary timing parameters. J Chem Phys 2008;128:154511.
93. Shemesh N, Ozarslan E, Komlosh ME, et al. From single-pulsed field gradient to double-pulsed field

gradient MR: gleaning new microstructural information and developing new forms of contrast in MRI. NMR Biomed 2010;23:757–80.
94. Smith SM, Jenkinson M, Johansen-Berg H, et al. Tract-based spatial statistics: voxelwise analysis of multi-subject diffusion data. Neuroimage 2006;31: 1487–505.
95. Kindlmann G, Westin CF. Diffusion tensor visualization with glyph packing. In: Proceedings Visualization/ Information Visualization. IEEE Transactions on Visualization and Computer Graphics 2006;12:1329–35.
96. Savadjiev P, Kindlmann G, Bouix S, et al. Local white matter geometry from diffusion tensor gradients. Neuroimage 2010;49:3175–86.